

Dual-wavelength efficient two-photon photorelease of glycine by π-extended dipolar coumarins

Maxime Klausen, Victor Dubois, Guillaume Clermont, Claire Tonnelé, Frédéric Castet, Mireille Blanchard-Desce

▶ **To cite this version:**

Maxime Klausen, Victor Dubois, Guillaume Clermont, Claire Tonnelé, Frédéric Castet, et al.. Dual-wavelength efficient two-photon photorelease of glycine by π-extended dipolar coumarins. Chemical Science, 2019, 10 (15), pp.4209-4219. 10.1039/C9SC00148D . hal-02416878

HAL Id: hal-02416878
https://hal.science/hal-02416878

Submitted on 17 Jan 2023

HAL is a multi-disciplinary open access archive for the deposit and dissemination of scientific research documents, whether they are published or not. The documents may come from teaching and research institutions in France or abroad, or from public or private research centers.

L'archive ouverte pluridisciplinaire **HAL**, est destinée au dépôt et à la diffusion de documents scientifiques de niveau recherche, publiés ou non, émanant des établissements d'enseignement et de recherche français ou étrangers, des laboratoires publics ou privés.

Journal Name

ARTICLE

Dual-wavelength efficient two-photon photorelease of glycine by π-extended dipolar coumarins.

Received 00th January 20xx,
Accepted 00th January 20xx

DOI: 10.1039/x0xx00000x

www.rsc.org/

Maxime Klausen,* Victor Dubois, Guillaume Clermont, Claire Tonnelé, Frédéric Castet, Mireille Blanchard-Desce*

Photolabile protecting groups (PPGs) releasing bioactive compounds upon two-photon excitation have emerged as increasingly popular tools to control and study physiological processes. Yet the limited two-photon photosensitivity of many cages is still a critical issue for applications. We herein report the design, synthesis and photophysical study of polarized extended coumarinyl derivatives which show large two-photon sensitivity (up to 440 GM) at two complementary wavelengths in the NIR spectral range. DFT calculations demonstrate that subtle tuning of polarization in the ground-state and confinement of the photo-induced intramolecular charge transfer upon excitation is responsible for enhancing two-photon absorption while maintaining large uncaging efficiency. These findings open a new engineering route towards efficient coumarinyl PPGs.

Introduction.

Among the light-responsive organic structures available, uncagers[1–3] represent key tools for biological and biomedical studies. These compounds act as photolabile protecting groups (PPGs) towards bioactive messengers, drugs[4–6] or neurotransmitters,[7–9] by masking their biological function. Suitable light irradiation then triggers the physiological response by releasing the free molecule with remarkable temporal and spatial control. In this respect, two-photon excitation (2PE) with near infrared (NIR) light provides significant advantages.[10–14] As opposed to UV-visible light, NIR wavelengths allow deeper penetration in tissues, reduced photo-damage and intrinsic 3D resolution. [10–14] The photolytic efficiency of a cage upon 2PE is quantified by its two-photon uncaging (2PU) cross-sections δ_u defined as $\delta_u = \sigma_2\Phi_u$; where σ_2 is the two-photon absorption (2PA) cross-section (in GM) and Φ_u the uncaging quantum yield.[15].

Until recently, the use of most cages described in the literature was somewhat limited for *in vivo* applications due to their low 2PU cross-sections (with δ_u^{max} values below 1 GM).[1,15] To overcome this limitation and avoid the use of deleterious excitation powers, two main engineering strategies have been developed in the last decade: the modification of the π-conjugated backbone of known cages[16–18] or the design of 2P sensitized tandem systems.[19,20] Both strategies led in several cases to innovative PPGs with δ_u values over a dozen GM. In addition, the recent design of spectrally orthogonal cages is also of major promise for applications in neurosciences.[21,22] In this regard, we have been interested in the design of cages with two complementary activation wavelengths, able to photorelease key amino-acids both at 700 nm and at 900 nm. Such cages would profitably complement the photochemical toolbox for neuroscientists. In particular, glycine (Gly) plays an important co-agonistic role, along with glutamate, in NMDA extrasynaptic receptors and is thus a key inhibitor neurotransmitter.[23]

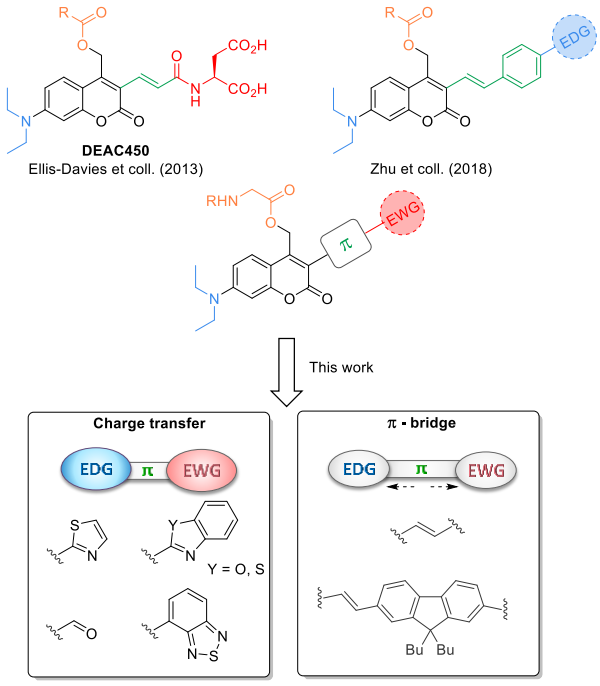


Figure 1. Recent evolution in the structure of π-extended coumarin PPGs and structures designed in the present work.

Univ. Bordeaux, Institut des Sciences Moléculaires (UMR5255 CNRS), 351 cours de la Libération, F-33405, Talence, (France)

† Footnotes relating to the title and/or authors should appear here.
Electronic Supplementary Information (ESI) available: [Experimental details of synthesis, photophysical and photochemical studies. DFT Calculations]. See DOI: 10.1039/x0xx00000x

Please do not adjust margins

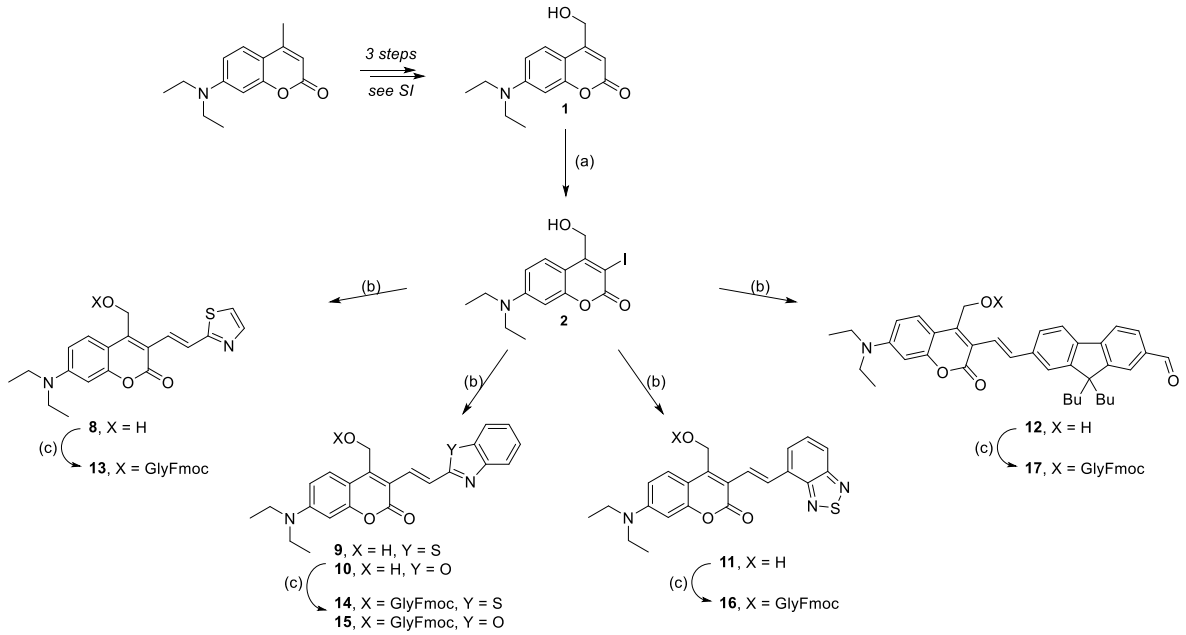
Please do not adjust margins

This motivated our effort towards the design of versatile and efficient Gly PPGs with very large 2P sensitivity (i.e. over 100 GM) at these two main working wavelengths where efficient uncaging of agonist (Glu) or antagonist (GABA) was previously accomplished.[21]

Among the variety of structures available, coumarinylmethyl PPGs are among the most widely studied molecular architectures.[1,24] The coumarin heterocyclic backbone, recognized as an efficient caging group,[9,24–26] can undergo a wide panel of chemical functionalization modulating its optical properties. Introducing an electron-withdrawing group (EWG) at the 3-position of the coumarin cage[21,27,28] was shown an influential way to red-shift both 1P and 2PA maxima respectively to the visible and the NIR,[27,29–31] as evidenced by DEAC450 (Figure 1).[21] Indeed, the design of DEAC450, which allows the photorelease of caged acids (Glu, GABA) with blue light irradiation (instead of UV irradiation for seminal compound DEAC) or upon 2P excitation at 900 nm, was a crucial step forward in the development of efficient cages of interest for neuroscientists. In addition, DEAC450 was demonstrated to show a very good uncaging quantum yield for glutamate release (39%), while DEAC had an uncaging quantum yield of 12%. This demonstrated that the extension of the coumarinyl moiety at the 3 position could indeed shift the absorption spectra towards the visible but also significantly affect the photolysis efficiency. Yet, albeit causing a substantial increase of uncaging quantum yield for amino-acid release, the acrylamide extension implemented in DEAC450 appeared to have limited effects on its 2PA properties, as indicated by the reported δ_u value (0.5 GM at 900 nm in physiological conditions).[21] This consideration led us to build our strategy on the increase of the 2PA response in new D-π-A extended DEAC derivatives, by modulating the intramolecular charge transfer in the ground-state to achieve optimum polarization leading to maximal 2PA[32] and (ii) further extending the π-conjugated system (Figure 1). A major questioning was to assess how the photochemistry of the original cage is affected by such changes, and to determine to what extent the electronic distribution of the PPG can be tuned in order to maximize the σ_2 without impeding the photolytic process. We thus prepared a small library of extended dipolar coumarinylmethyl derivatives bearing dedicated electron-withdrawing end-groups (EWG) at the 3-position (Figure 1). To fulfil this role, we chose nitrogen-based aromatic heterocycles such as thiazoles and derivatives[33] (Figure 1). These new PPGs were then used to cage and release Fmoc-protected glycine with two primary goals: (i) performing a model study of the parameters regulating their photolytic efficiency, and (ii) enlightening the experimental results with DFT calculations in pursuance of rationale in the design of such coumarinyl PPGs.

Results and discussion.

Design and synthesis. The synthetic layout of the new "free" DEAC cages involves three main challenges: the introduction of the fundamental 4-hydroxymethyl group on the aminocoumarin skeleton, the synthesis of the vinyl-acceptor moiety, and finally functionalization at the 3-position with the double bond. The formation of the alcohol **1** was achieved starting from the commercially available 7-diethylamino-4-methylcoumarin using an original pathway involving the formation of an intermediate enamine[34] which was found to be much cleaner, more efficient and convenient than the usual selenium dioxide oxidation[35] in our hands (Scheme S1). The extension of the π-conjugated system at the 3-position of the coumarin scaffold was then achieved by Heck cross-coupling using the iodinated substrate **2**.



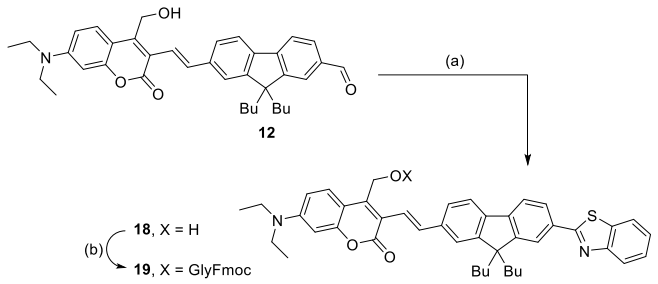
Scheme 1. Synthesis of extended polarized coumarin cages. Reagents and conditions: (a) NIS, $BF_3.Et_2O$, $CHCl_3$, 0 °C to r.t. (70%). (b) **3-7**, $Pd(OAc)_2$, *n*-Bu_4NCl, LiCl, $NaHCO_3$, DMF, 130°C (**8**, 90%; **9**, 96%; **10**, 92%, **11**, 76%; **12**, 89%). (c) Fmoc-Gly-OH, EDC.HCl, DMAP (cat.), CH_2Cl_2, r.t. (**13**, 52%; **14**, 59%; **15**, 69%; **16**, 58%; **17**, 84%).

This journal is © The Royal Society of Chemistry 20xx

Please do not adjust margins

Journal Name

ARTICLE



Scheme 2. Synthesis of cage **19**. Reagents and conditions: (a) 2-Aminothiophenol hydrochloride, DMF, 120 °C. (42%). (b) Fmoc-Gly-OH, EDC.HCl, DMAP (cat.), (64%).

Iodination of the free alcohol **1** was successfully performed in good yield and large scale by using *N*-iodosuccinimide in the presence of a strong Lewis acid, which provided for a highly activated source of electrophilic iodine (Scheme 1).

The vinyl-based electron-accepting modules were synthesized by different procedures, depending on the synthon. 2-vinylbenzothiazole, -benzoxazole, and -benzothiadiazole derivatives (**4**, **5** and **6**) were synthesized by Suzuki coupling with potassium vinyl trifluoroborate.[36,37] 2-vinylthiazole (**3**) and 9,9-dibutyl-7-vinyl-9*H*-fluorene-2-carbaldehyde (**7**) were obtained by Wittig reactions starting from the corresponding aldehydes (see SI). Heck reaction using Jeffery conditions[21,38] between intermediates **2** and **3-7** finally afforded compounds **8-12** in good to excellent yields, often without extensive purification (Scheme 1).

Eventually, condensation of intermediate **12** with 2-aminothiophenol hydrochloride yielded without additional protection step a fluorene-containing derivative **18**, which was then esterified with Fmoc-Gly-OH to yield the final PPG **19** (Scheme 2).

Photophysical Properties. With all compounds in hands, the photophysical one- and two-photon absorption properties were investigated. Dimethylsulfoxide was chosen as solvent for the photophysical study due to its high polarity (thus closer to water than low-polarity organic solvents) reasonable viscosity (favourable to fluorescence) and optimal solubility of the whole series of compounds.

All new PPGs show intense absorption in the visible and fluorescence properties (see spectra in SI). Experimental data are summarized in Table 1. As expected, the extension of the π-conjugated system with a vinyl-acceptor group at the 3-position induced a marked bathochromic and hyperchromic shift in absorption and red-shifted emission as compared to DEAC. This trend is amplified by the addition of the fused benzenic ring in the heterocyclic end-group, responsible for an additional 13 to 28 nm red-shift of the absorption band from thiazole to benzothiadiazole compared to DEAC450. A significant hyperchromic effect is also observed, as supported by the 40% enhancement of the ε^{max} value in **14** compared to DEAC450. Interestingly, the elongated fluorenyl compounds **17** and **19** showed an intermediary behaviour, with absorption coefficients falling in the same range as the vinyl derivatives **14** and **15** but with less marked bathochromic shifts of their absorption/emission compared to DEAC450. Among the series, compound **16** which bears the strongest EWG shows a singular behaviour, with an absence of hyperchromic effect but a marked red-shifted and much weaker emission compared to DEAC450. This suggests that strong photo-induced ICT takes place after excitation prior to emission. This leads to a strongly polarized emissive excited-state which is stabilized by polar environments. This is confirmed by the pronounced positive fluorescent solvatochromic behaviour of this compound, not observed in other derivatives (see SI), and further demonstrated by DFT calculations (*vide infra*).

Table 1. Photophysical (1P and 2P) properties of **13-17**, **19** and reference compound DEAC450 in DMSO.

Cpd	λ_{abs}^{max} (nm)	ε^{max} ($M^{-1}.cm^{-1}$)	λ_{em}^{max} (nm)	Φ_f	λ_{2PA}^{max} (nm)	σ_2^{max} c) (GM)
DEAC450	444	$3.4\ 10^4$	523	0.82[a)]	890	123
13	457	$3.6\ 10^4$	541	0.95[a)]	950 700	164 191
14	472	$4.7\ 10^4$	562	0.87[a)]	970 710	371 441
15	467	$4.6\ 10^4$	552	0.92[a)]	970 700	267 367
16[d)]	472	$3.3\ 10^4$	692	0.13[b)]	970 730	215 191
17	457	$4.6\ 10^4$	553	0.56[a)]	940 730	147 621
19	458	$4.2\ 10^4$	547	0.59[a)]	940 730	143 988

[a)] Fluorescence quantum yield (standard: fluorescein in 0.1M NaOH (Φ_f=0.9)). [b)] Fluorescence quantum yield (standard: rhodamine 6G in EtOH (Φ_f=0.94)) [c)] 2PA cross-section at λ_{2PA}^{max} derived from 2PEF experiments in DMSO. [d)] 2PA measurement performed in toluene.

Uncaging properties. One-photon uncaging efficiencies were then assessed by irradiating samples of the new compounds and reference PPG at 455 nm, and monitoring unambiguously the release rate of the caged Fmoc-Gly-OH upon irradiation by ^{1}H NMR (Figure 2a). For the sake of comparison, we performed the photolysis in a CD_3CN/D_2O (9/1, v/v) mixture which is commonly used in the literature.[27,39–41] In this model study, we also decided to preserve the protecting group on the glycine ester, which quite conveniently allowed the quantitation of the released species (rather than degradation of the cage)

This journal is © The Royal Society of Chemistry 20xx

Please do not adjust margins

either by monitoring the CH_2 of the amino-acid itself or that of the Fmoc protecting group.

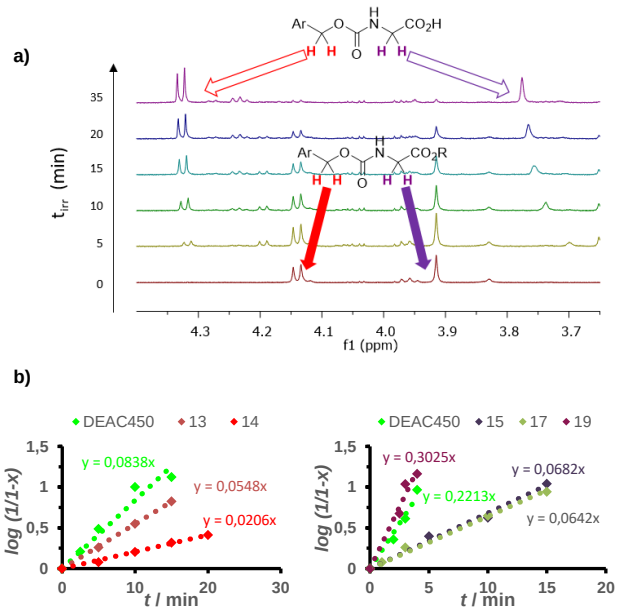


Figure 2. a) Example of evolution of the ^{1}H NMR spectrum of the coumarinyl PPG **14** upon excitation at 455 nm in CD_3CN/D_2O (9/1, v/v), and kinetic follow-up of the photorelease. b) Comparative kinetics of photolysis upon irradiation at 455 nm of the reference PPG (DEAC450) and new polarized PPGs in CD_3CN/D_2O at 0.7 mM (left) or at 0.25 mM (right); derived from ^{1}H NMR experiments.

First order kinetics were observed in all cases (Figure 2b), allowing the derivation of the one-photon uncaging sensitivity $\varepsilon_{455}Q_u^{rel}$ from the slope values compared to those of **DEAC450-Gly** irradiated in the exact same conditions (see SI),[42] and subsequently, the ratio of the relative uncaging quantum yield Q_u^{rel} value toward the reference uncaging quantum yield Φ_u^{ref} (Table 2).

All compounds except **19** proved to have lesser uncaging rates than DEAC450-Gly. Yet, the relative uncaging quantum yields still reached 20% for compound **13**, which remains higher than most PPGs described so far. A marked reduction of the Q_u^{rel} value was revealed by benzo-compounds **14** and **15** whose efficacy is largely reduced (by about 50 % compared to compound **13**) indicating that the presence of the fused ring on the EWG is detrimental to the photorelease efficiency. Most markedly, compound **16** did not proceed to uncaging of glycine upon excitation, and proved unsuitable for uncaging applications.

Table 2. Photochemical (1P and 2P) properties of **13-17**, **19** and reference compound DEAC450 in aqueous acetonitrile.

Cpd	ε_{455nm} ($M^{-1}.cm^{-1}$)	Q_u^{rel}/Φ_u^{ref} a)	Q_u^{rel} b)	ε_u^{max} c) ($M^{-1}.cm^{-1}$)	λ_{2PA}^{max} (nm)	δ_u^{max} d) (GM)
DEAC450	$3.2\ 10^4$	1	0.39	13.10^3	890	48
13	$3.6\ 10^4$	0.50	0.20	$7.8.10^3$	950 700	32 37
14	$4.1\ 10^4$	0.21	0.08	$4.0.10^3$	970 710	30 36
15	$4.1\ 10^4$	0.24	0.09	$4.5.10^3$	970 700	25 35
16	$3.0\ 10^4$	< 0.02	-	-	970 730	- -
17	$4.6\ 10^4$	0.23	0.09	$4.2.10^3$	940 730	13 56
19	$4.3\ 10^4$	1.14	0.45	21.10^3	940 730	64 442

a) Ratio of uncaging quantum yield values derived from comparative 1P photolysis experiments in CD_3CN/D_2O (9/1, v/v) at 455 nm. b) Uncaging quantum yield values calculated using Φ_u^{ref}=0.39 for DEAC450-[Gly]. c) One-photon uncaging sensitivity at λ^{max}. d) Two-photon uncaging sensitivity at λ_{2PA}^{max} estimated from comparative 1P photolysis experiments and 2PEF measurements.

The benzothiadiazolyl end-group, the strongest EWG in the series, is clearly detrimental to photolysis, indicating that a strongly polarized excited-state and marked photo-induced ICT is unfavourable for this specific purpose. This behaviour was further confirmed by DFT calculations, which revealed that the elongation of the C-O bond upon excitation in compound **16** is 2-3 times smaller than in the other compounds (*vide infra*).

Surprisingly, a different behaviour was observed for extended derivatives **17** and **19** bearing a fluorenyl unit in the conjugated π-connector. While the aldehyde derivative **17** displays a moderate but still reasonable Q_u^{rel} of 9%, the benzothiazolyl derivative **19** shows an uncaging efficiency comparable to that of DEAC450 (Table 2). Indeed, **19** proved slightly faster than reference compound DEAC450 upon 1P photolysis, leading to a Q_u^{rel} value of 45%, whereas its vinyl counterpart **14** displayed a Q_u^{rel} value of only 8%. This suggests that the introduction of an intermediate fluorenyl π-bridge in compound **19** is responsible for a redistribution in the electron density,[43] favouring significant increase of Φ_u.

Dark stability. Importantly, whereas amino acid esters have sometimes been reported unstable in aqueous media,[9] all of our new compounds proved to be stable towards dark hydrolysis in this photolysis medium, as no significant degradation of the chromophores was observed after several days in solution in the dark at room temperature (see SI).

DFT calculations. DFT calculations conducted at the M06-2X/6-311G(d) level[44] were performed to gain further insight into the polarization and electronic structures of the ground and first excited states of these derivatives. Table 3 reports the vertical spectroscopic properties of the investigated compounds, together with the electric dipoles of the S_0 and S_1 states (μ_0 and μ_1^{vert}) and their difference ($\Delta\mu_{01}^{vert}$). The computed absorption spectra are reported in SI. In every compound, the

This journal is © The Royal Society of Chemistry 20xx

Please do not adjust margins

first optically allowed excited state (S_1) is dominated by a HOMO→LUMO π–π^* excitation. Excitations implying the HOMO-1 and LUMO+1 also contribute to the $S_0 \rightarrow S_1$ transition in extended derivatives **17** and **19** (see SI for details). The isodensity surfaces of the frontier orbitals are sketched in Figure 3 and show that both HOMO and LUMO are delocalized along the conjugated part of the molecule.

Table 3. Vertical transition energy (ΔE_{01}, eV) and wavelength (λ_{01}, nm), as well as, oscillator strength (f_{01}), transition dipole moment (μ_{01}, D), ground state and excited state dipole moments (μ_0 and μ_1^{vert}, D), dipole moment variation ($\Delta\mu_{01}^{vert}$, D), charge transferred upon excitation (q^{CT}, |e|), and charge transfer distance (d^{CT}, Å), calculated at the TDDFT/M06-2X/6-311G(d) level in acetonitrile.

Cpd	λ_{exp}	ΔE_{exp}	ΔE_{01}	λ_{01}	f_{01}	μ_{01}	μ_0	μ_1^{vert}	$\Delta\mu_{01}^{vert}$	q^{CT}	d^{CT}
DEAC450	444	2.793	3.125	397	1.39	10.81	6.76	14.99	8.25	0.584	2.940
13	457	2.713	2.935	422	1.70	12.36	6.38	12.41	6.70	0.540	2.581
14	472	2.627	2.874	431	1.87	13.09	7.52	14.89	8.09	0.568	2.967
15	467	2.655	2.902	427	1.84	12.94	8.05	14.97	7.59	0.566	2.789
16	472	2.627	2.941	422	1.55	11.78	12.92	22.51	10.53	0.581	3.775
17	457	2.713	3.012	412	2.23	13.99	14.39	21.28	7.18	0.551	2.714
19	458	2.707	3.004	413	2.57	15.02	11.22	17.10	6.35	0.544	2.433

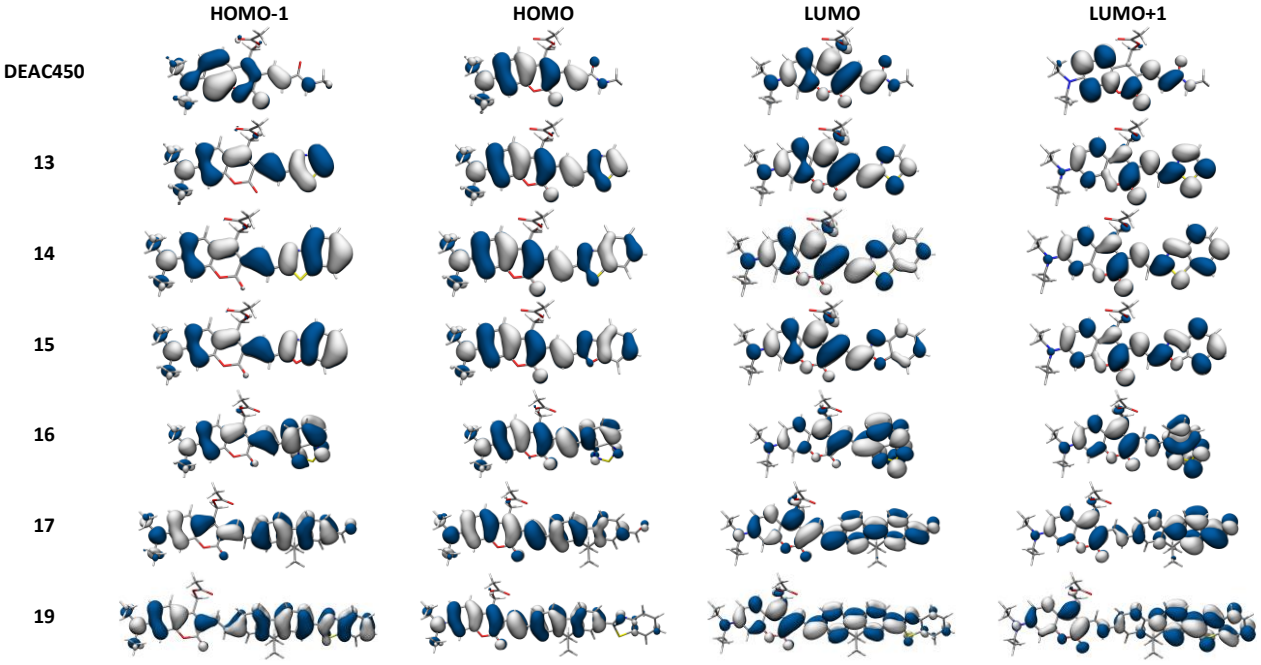


Figure 3. Graphical representations of the frontier orbitals of the investigated compounds, calculated at the IEFPCM:M06-2X/6-311G(d) level

As shown in Table 3, TDDFT calculations qualitatively reproduce the red-shifts measured experimentally upon substitution at the 3-position of the coumarin cage. With respect to the reference compound DEAC450, adding a fused benzenic ring on the terminal EWG (from thiazole in compound **13,** to benzothiadiazole in compound **14**) results in computed bathochromic shifts of 0.08 and 0.17 eV, respectively, which compares well with the measured bathochromic displacements of 0.19 and 0.25 eV. Besides, the associated increase of the oscillator strength is also in accordance with the hyperchromic shift observed experimentally. The absence of further red-shift of the absorption band in the more extended compounds **17** and **19** is similarly well reproduced. Finally, TDDFT calculations support the specific spectroscopic properties of compound **16**, which shows a marked bathochromic but no significant hyperchromic shift with respect to DEAC450. These spectral evolutions can be traced back to the magnitude of the photo-induced ICT, which is quantified by the dipole moment variation $\Delta\mu_{01}^{vert}$. In particular, the largest $\Delta\mu_{01}^{vert}$ value is found for **16**, which is mostly related to an increased charge transfer distance d^{CT} in this compound. The total charge transferred is however of similar magnitude for all compounds (Table 3).

In order to gain better insight into the difference of photochemical behavior between derivatives, relaxed geometries of the S_1 states were calculated. Table 4 reports the photo-induced elongation of the C-O single bond connecting the glycine ester to the coumarinylmethyl protecting moiety, defined as the difference between the C-O distances issued from S_1 and S_0 gas phase optimizations ($\Delta_{CO} = d_{CO}^{S1} - d_{CO}^{S0}$). The adiabatic ($E_{adia}$) and 0-0 energies ($E_{0-0}$) are also reported, as well as the excited-state dipole moment (μ_1^{opt}) and photo-induced dipole moment variation ($\Delta\mu_{01}^{opt}$) calculated using relaxed gas phase geometries

Please do not adjust margins

($\Delta\mu_{01}^{opt} = \mu_1^{opt} - \mu_0$). Finally, these last two quantities were further refined to account for solvent effects, by performing IEF-PCM:TD-DFT single-point calculations (Table 4, last columns).

We note a slight elongation of the C-O bond in all compounds in relaxed excited state S_1 from which photochemistry and fluorescence occur. It is interesting to note that compound **16** exhibits the smallest Δ_{CO} value within the series (more than twice smaller than that of DEAC450), together with the largest excited-state dipole moment (μ_1^{opt+s} = 23 D, about twice larger than that of DEAC450), and photo-induced dipole moment variation. This result confirms that the large photo-induced ICT occurring within this compound is detrimental to its uncaging efficiency. On the other hand, all other new derivatives (**13-15**, **17**, **19**) show similar Δ_{CO} values, close to that of DEAC450.

Neither the excited dipole moments values, nor the variation of dipole moment appear to show direct correlation with uncaging efficiency. However, closer examination of HOMO-LUMO[43] does reveal interesting features. For compounds **13-16**, photo-induced ICT extends to the EW end-groups; the sharpest effect being observed for compound **16** which bears the strongest terminal EWG. In contrast, the photo-induced ICT remains mostly limited to the extended conjugated system in compound **17** and **19**. Furthermore, comparison of the d^{CT} values of these two compounds (Table 3) indicates that extension of the photo-induced ICT leads to a decrease of uncaging efficiency (Figure 4).

To further investigate the origin of difference in uncaging efficiency between derivatives **13-17**, and **19**, calculation of the carbocations that are presumed key intermediates in the photolysis mechanism[45,46] was undertaken (see SI). Starting from the relaxed geometries of the S_1 photo-activated state, rigid energy scans were first performed by elongating progressively the C-O bond up to the photolytic dissociation limit, in order to evaluate the bond dissociation energy (BDE) in the excited electronic state. Geometry optimizations of the carbocations were also conducted in the S_0 state to compare their relative stability with respect to the parent coumarinyl derivatives (see SI). These two series of calculations led to very similar conclusions. Interestingly, fluorenyl-based compounds **17** and **19** give rise to the lowest BDE and to the most stable carbocations within the series whereas compounds **14** and **15** lead to the largest BDE and to the least stable carbocations. We note however that the compound DEAC450 falls out of the correlation (as was the case for d_{CT}) suggesting that different mechanisms might be involved.

Table 4. Photo-induced elongation of the C-O bond (Δ_{CO}, Å), adiabatic (E_{adia}, eV) and 0-0 energies (E_{0-0}, eV), excited state dipole moment (μ_1^{opt}, D) and dipole moment variation ($\Delta\mu_{01}^{opt}$, D), obtained from the gas phase geometries of the S_1 and S_0 states both optimized at the M06-2X/6-311G(d) level.

	Gas					Acetonitrile	
	Δ_{CO}	E_{adia}	E_{0-0}	μ_1^{opt}	$\Delta\mu_{01}^{opt}$	μ_1^{opt+s}	$\Delta\mu_{01}^{opt+s}$
DEAC450	0.018	3.309	3.221	9.11	4.27	13.97	7.26
13	0.015	3.061	2.987	6.85	2.60	11.05	5.37
14	0.013	2.983	2.909	8.19	2.95	13.79	6.98
15	0.014	3.021	2.944	7.75	2.23	13.60	6.23
16	0.008	2.895	2.828	15.13	5.90	22.99	10.99
17	0.015	2.971	2.907	13.37	2.85	20.48	6.97
19	0.014	2.928	2.863	9.80	2.61	16.35	6.53

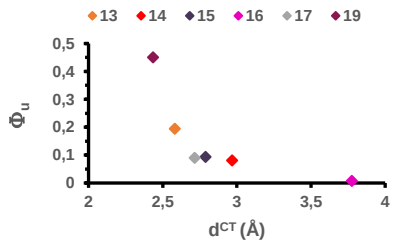


Figure 4. Correlation between the extent of photo-induced ICT (d^{CT}) and the relative uncaging quantum yields Q_u^{rel} in compounds **13-17** and **19**.

Two-photon absorption

The two-photon absorption spectra of the new PPGs **13-17** and **19** were determined by conducting two-photon excited fluorescence experiments (2PEF) in DMSO solution (Table 1). DMSO was chosen as a viscous non-protic solvent, thus promoting fluorescence (Table 1) and allowing accurate and reliable 2PA measurements. At opposite, the presence of water, although beneficial to photorelease, logically reduces fluorescence.

All compounds exhibit *two intense 2PA bands* in the spectral range of interest (690-1000 nm) which is not the case of DEAC450 (Figure 5a-b) which is blue-shifted compared to the series of compounds investigated.

An intense band located at about twice the maximum wavelength of 1PA (see SI) is observed around 940-970 nm with maximum 2PA cross-sections varying between 140 and 370 nm. Firstly, we note that the maximum 2PA cross-section measured for DEAC450 in DMSO (123 GM at 890 nm) is almost two orders of magnitude larger than the one derived from δ_u and Φ_u values reported in buffered water (i.e., 1.3 GM). This difference may partly be related to solvent effect as water may significantly affect 2PA. We note that 2PA measurements

This journal is © The Royal Society of Chemistry 20xx

Please do not adjust margins

reported earlier for coumarin **1**, a 4-methyl analogue of DEAC yielded a maximum 2PA cross-section in ethanol of 103 GM at 755 nm.[47] Our measurements gave a σ_2^{max} value of 44 GM at 760 nm for DEAC450 in DMSO (see SI), illustrating the influence of the environment and electric field effects on 2PA. These values are consistent with the larger maximum 2PA cross-section measured for extended DEAC450 at 890nm (123 GM). The almost two-orders of magnitude smaller σ_2^{max} value derived from the reported δ_u value (1.3 GM) suggests that formation of dimers of DEAC450 may occur in the aqueous environment where δ_u measurements were conducted. Indeed formation of dimers of dipolar chomophores may significantly reduce 2PA properties.[48]

Secondly, we observe that all new derivatives show red-shifted and more intense 2PA responses than DEAC450 (Figure 5). While compound **13** shows slightly larger σ_2^{max1} value (165 GM instead of 123 GM) than DEAC450, the additional fused benzenic ring on the EWG in **14** and **15** induces a two to three fold enhancement of this value (i.e., 370 GM and 270 GM respectively). In contrast, the ε^{max} values were found to increase by only 40 %, evidencing stronger effect on 2PA. As a result, extended coumarin derivatives **14** and **15** show unprecedented 2PA responses at 970 nm, over one order of magnitude larger than coumarin fluorochromes commonly used in bioimaging.[49] We also note that compound **14** shows a 37 % larger σ_2^{max1} value as compared to compound **15**, confirming that the benzothiazole EWG leads to larger 2PA responses than benzoxazole.

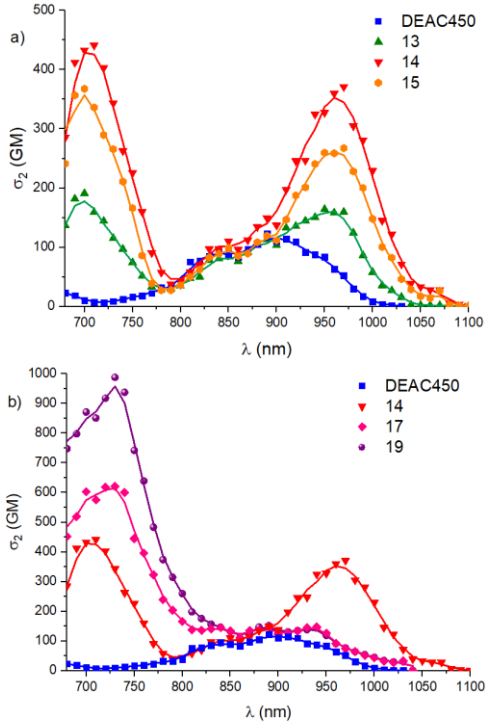


Figure 5. Comparison of the 2PA spectra of a) vinyl derivatives **13-15** and **DEAC450** in DMSO; b) dipolar compounds **14**, **17**, **19** and **DEAC450** in DMSO.

Compound **16**, which bears the strongest EWG in the series and shows the largest polarization for derivatives of similar length (see Table 3, μ_0=12.9 D), shows a broader and weaker 2PA band than compounds **14** and **15**, with a σ_2^{max1} reaching 215 GM. This indicates that derivatives **14** and **15** are close to optimum polarization (μ_g=7.5 and 8.0 D) leading to maximal 2PA, while compound **16** is most probably too polarized (i.e. over optimum ICT in the ground state).[32] In contrast, extended derivatives **17** and **19** show σ_2^{max1} values which are similar and only slightly larger than that of DEAC450 (i.e. 150 and 140 GM). Hence the presence of the fluorenyl bridge is detrimental to the low energy 2PA band, in relation with lesser ICT in the ground state due to the higher cost associated with charge separation along the full length of molecules **17** and **19**.[32]

Strikingly, a second and even more intense higher energy band is observed around 700-730 nm for all new PPGs (Figure 5). This higher energy band is strongly 2P allowed and corresponds to a strongly 1P allowed excited-state only for extended compounds **17** and **19** (see SI). The addition of a fused benzenic ring in the terminal EWG induces a significant increase of the σ_2^{max2} bands (Figure 5a), as indicated by the comparison of compounds **13** and **14**. The nature of the heterocyclic moiety, also significantly influences the σ_2^{max2} values as witnessed by the 19 % increase observed in the benzothiazole PPG **14** (440 GM) compared to its benzoxazole counterpart **15** (370 GM).

Again, compound **16** shows a different behaviour. Due to its far-red/NIR emission in DMSO, which prevented access to the higher energy band located around 700 nm by 2PEF measurements, 2PA measurements were conducted in toluene (a solvent in which compound **16** emits in the visible, see SI). The resulting measurements in the full 700-1100 nm range do reveal a second high energy band, as in the other dipolar compounds. As was the case for the low-energy 2PA band, the σ_2^{max2} value (around 200 GM, see Table 1) is again much lower than for analogues **14** and **15** of similar size.

In contrast, a spectacular influence of the fluorenyl bridge is evidenced in compounds **17** and **19** (Figure 5b). Unlike their lower-energy 2PA bands, the transitions located at 730 nm show very high maxima, with a σ_2^{max2} value twice larger for the benzothiazolyl derivative **19** than for its shorter analogue **14**. With a remarkable σ_2^{max} value of 990 GM, compound **19** also exhibits a 60% higher 2PA cross-section than its aldehyde counterpart **17**, hereby evidencing the role of the EWG in the phenomenon. The differences in the 2PA higher energy maxima of these three compounds can be related to the nature of the second optically allowed absorption band, as rationalized by DFT calculations (see SI). In compound **19**, the $S_0 \rightarrow S_2$ transition is strongly optically allowed (as indicated by its large oscillator strength, f_{02} = 0.55), and associated to a large photo-induced dipole variation ($\Delta\mu_{02}$ = 6.89 D). In compound **17**, absorption towards the second bright excited state (which corresponds to the $S_0 \rightarrow S_3$ transition) also gives rise to a significant reorganization of the electron density ($\Delta\mu_{03}$ = 8.58 D) but with a twice-smaller intensity (f_{03} = 0.29). In **14**, the intensity of the $S_0 \rightarrow S_2$ transition is much weaker (f_{02} = 0.13) and associated to a negligible $\Delta\mu_{02}$ value (0.46 D).

Please do not adjust margins

Two-photon uncaging

As discussed above, the nature of the EWGs as well as the presence of a conjugated linker significantly affects both the 2PA response and the uncaging efficiency. In particular optimum polarization leads to very large 2PA responses both at 970 nm (370 and 270 GM for compounds **14** and **15** respectively) and 700 nm (440 GM and 370 GM for compounds **14** and **15**) while insertion of the fluorenyl unit in the conjugated system leads to very large 2PA responses at 730 nm. Besides, the extension of electronic redistribution (d^{CT}) is detrimental to the uncaging efficiency. Hence both tuning of ICT in the ground-state *and* limitation of electronic redistribution upon excitation are key parameters which control the two-photon sensitivity ($\delta_u=\sigma_2*\Phi_u$).

Extrapolated 2P uncaging sensitivities derived from previous measurements of 2PA cross-section and uncaging quantum yield are reported in Table 2. Although the nature of solvent does affect the 2PA response (*vide supra*), these values give consistent trends among the series of derivatives and allow direct comparison with DEAC450. For PPGs of the vinyl series **13**-**15**, the increase in σ_2^{max} is somewhat counterbalanced by a drop of Q_u^{rel}. Yet, in all three cases, the calculated δ_u values reach about 35 GM for irradiation in the higher energy band *and* 25-30 GM for the lowest energy band. These values are only slightly smaller than that extrapolated for DEAC450;[50] their main advantage being that they can be used either at 700-720 nm (like DEAC or MNI)[8,25] or at 950 nm, thus offering improved penetration depth and interesting sequential alternatives for *in vivo* experiments. As such they represent promising uncaging tools to be used in conjunction with complementary cages that would photorelease antagonists and coagonists of Gly.

Eventually, thanks to its very large 2PA cross-sections in the 700-750 nm range (over 700 GM) combined with a slightly improved uncaging quantum yield with respect to DEAC450, the extended fluorenyl derivative **19** shows a record estimated δ_u of about 440 GM at 730 nm. To confirm the potential use of this new derivative in 2P uncaging experiments, we performed the irradiation of **19** at both 2P maxima for 7 h in similar conditions, and compared the conversion of the photolysis reaction with two appropriate standards, *i.e.* DEAC at 730 nm and DEAC450 at 940 nm (Figure 6). Irradiation of the samples at 730 nm clearly evidenced a sevenfold enhancement in 2P photosensitivity between compound **19** and parent DEAC, in agreement with δ_u values derived from 1P uncaging studies and 2PEF measurements using the $\delta_u=\sigma_2*\Phi_u$ relationship. Furthermore, we observe a major enhancement (by about a factor 8) of the 2P sensitivity of compound **19** at 730 nm compared to is 2P photosensitivity at 940 nm. Again, this is consistent with the relative δ_u values derived at 730 and 940 nm for this compound, thus validating our study. Finally, comparative irradiation of DEAC450 and compound **19** at 940 nm indicate an enhancement of 2P sensitivity by over a factor 2, as anticipated from comparison of δ_u values of both compounds derived from 1P uncaging and 2PEF studies.

This study demonstrates that by tuning ICT in the ground state and electronic redistribution in the photoactive excited state, we could indeed enhance both uncaging efficiency and 2PA properties. As a result, coumarin derivative **19** shows unprecedented 2P sensitivity at 730 nm while retaining similar 2P sensitivity at 890 nm as DEAC450. In contrast, shorter derivative **13** shows similar 2P sensitivity, comparable to DEAC450, at *two* complementary wavelengths (700 and 950 nm).

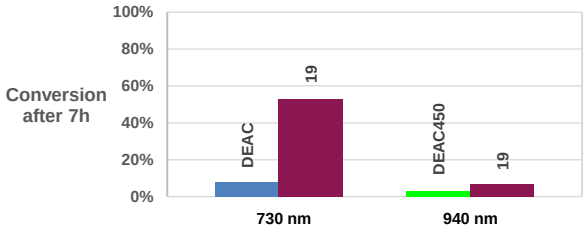


Figure 6. Comparative histogram showing the conversion of the uncaging reaction (Gly release) after 7 h of two-photon irradiation at 730 and 940 nm in similar conditions (1.2 mL, 1W).

Conclusion

This work unveils a new direction towards dipolar coumarin cages with unique two-photon uncaging sensitivity. The combination of experimental spectroscopic investigation with computational chemistry revealed surprising structure-property relationships where subtle tuning of the ground-state polarization and containment of photo-induced redistribution in the excited state triggers both the photolysis and the 2PA ability. These achievements open the route to unique opportunities in neurosciences. Further work along that direction is currently in progress.

Conflicts of interest

The authors declare no conflicts of interest.

Acknowledgements

MBD gratefully acknowledges the Conseil Régional d'Aquitaine for funding ("Chaire d'Accueil d'excellence" grant). We also acknowledge the University of Bordeaux for fellowships to MK and VD. CT thanks the LAPHIA centre of excellence, managed by the ANR under the initiative of excellence (IdEx) program (reference ANR-10-IDEX-0003-02), for her postdoctoral fellowship. Computer time was provided by the Pôle Modélisation HPC facilities of the Institut des Sciences Moléculaires, co-funded by the Nouvelle Aquitaine region.

Computational methods

The geometry of the ground (S_0) and first singlet excited (S_1) states were optimized in the gas phase in the framework of the Density Functional Theory (DFT) using the M06-2X exchange-correlation functional[44] and the 6-311G(d) basis set. All structures were characterized as real minima of the potential energy surface on the basis on their positive

This journal is © The Royal Society of Chemistry 20xx

Please do not adjust margins

Please do not adjust margins

vibrational force constants. Ground state optimized geometries were used to compute the vertical transition energies and excited state properties by employing the Time-Dependent Density Functional Theory (TD-DFT) at the M06-2X/6-311G(d) level. Solvent effects (acetonitrile) were taken into account in these calculations by using the Integral Equation Formalism of the Polarizable Continuum Model (IEF-PCM).[51] The photo-induced charge transfer was analyzed on the basis of vertical electronic transitions, by considering the difference $\Delta\mu_{01}^{vert}$ in the electric dipoles of the S_0 and S_1 states. Using the approach reported in refs [52] and [53], $\Delta\mu_{01}^{vert}$ was further decomposed as $\Delta\mu_{01}^{vert} = q^{CT} \times d^{CT}$, where q^{CT} is the photo-induced charge transfer, *i.e*. the global amount of charge transferred upon light excitation, and d^{CT} is the distance over which this charge is transferred.

Then, the effects of structural relaxation on the electronic structure of the S_1 state were addressed. The adiabatic energies, defined as the energy difference of the S_1 and S_0 states in their respective minimum ($E_{adia} = E_{S1}^{opt} - E_{S0}^{opt}$), were calculated on the basis of the gas phase geometries. The 0-0 energies were then evaluated as the sum of the adiabatic contribution and the difference of zero-point vibrational energy (ZPVE) between S_1 and S_0 ($E_{0-0} = E_{adia} + \Delta E_{ZPVE}$). Finally, IEF-PCM:TD-DFT single-point calculations in acetonitrile were performed on the (gas phase) relaxed geometries of S_1, to evaluate the excited-state dipole moment and photo-induced dipole moment variation $\Delta\mu_{01}^{opt+s}$ accounting for geometrical relaxation effects. All calculations were performed using the Gaussian 09 package.[54]

Notes and references

1 P. Klán, T. Šolomek, C. G. Bochet, A. Blanc, R. Givens, M. Rubina, V. Popik, A. Kostikov and J. Wirz, Photoremovable Protecting Groups in Chemistry and Biology: Reaction Mechanisms and Efficacy, *Chem. Rev.*, 2013, **113**, 119–191.

2 G. C. R. Ellis-Davies, Caged compounds: photorelease technology for control of cellular chemistry and physiology, *Nat Meth*, 2007, **4**, 619–628.

3 H. Yu, J. Li, D. Wu, Z. Qiu and Y. Zhang, Chemistry and biological applications of photo-labile organic molecules, *Chem. Soc. Rev.*, 2010, **39**, 464–473.

4 R. Horbert, B. Pinchuk, P. Davies, D. Alessi and C. Peifer, Photoactivatable Prodrugs of Antimelanoma Agent Vemurafenib, *ACS Chem. Biol.*, 2015, **10**, 2099–2107.

5 D. E. McLain, A. C. Rea, M. B. Widegren and T. M. Dore, Photoactivatable, biologically-relevant phenols with sensitivity toward 2-photon excitation, *Photochem. Photobiol. Sci.*, 2015, **14**, 2151–2158.

6 Y. Venkatesh, S. Karthik, Y. Rajesh, M. Mandal, A. Jana and N. D. P. Singh, Three-Arm, Biotin-Tagged Carbazole–Dicyanovinyl–Chlorambucil Conjugate: Simultaneous Tumor Targeting, Sensing, and Photoresponsive Anticancer Drug Delivery, *Chem. Asian J.*, 2016, **11**, 3482–3486.

7 E. M. Callaway and L. C. Katz, Photostimulation using caged glutamate reveals functional circuitry in living brain slices, *Proc. Natl. Acad. Sci. U.S.A.*, 1993, **90**, 7661–7665.

8 M. Matsuzaki, G. C. R. Ellis-Davies, T. Nemoto, Y. Miyashita, M. Iino and H. Kasai, Dendritic spine geometry is critical for AMPA receptor expression in hippocampal CA1 pyramidal neurons, *Nat Neurosci*, 2001, **4**, 1086–1092.

9 T. Furuta, S. S.-H. Wang, J. L. Dantzker, T. M. Dore, W. J. Bybee, E. M. Callaway, W. Denk and R. Y. Tsien, Brominated 7-hydroxycoumarin-4-ylmethyls: Photolabile protecting groups with biologically useful cross-sections for two photon photolysis, *PNAS*, 1999, **96**, 1193–1200.

10 F. Terenziani, C. Katan, E. Badaeva, S. Tretiak and M. Blanchard-Desce, Enhanced Two-Photon Absorption of Organic Chromophores: Theoretical and Experimental Assessments, *Adv. Mater.*, 2008, **20**, 4641–4678.

11 M. Pawlicki, H. A. Collins, R. G. Denning and H. L. Anderson, Two-Photon Absorption and the Design of Two-Photon Dyes, *Angew. Chem. Int. Ed.*, 2009, **48**, 3244–3266.

12 S. Yao and K. D. Belfield, Two-Photon Fluorescent Probes for Bioimaging, *European Journal of Organic Chemistry*, 2012, **2012**, 3199–3217.

13 D. Kim, H. G. Ryu and K. H. Ahn, Recent development of two-photon fluorescent probes for bioimaging, *Org. Biomol. Chem.*, 2014, **12**, 4550–4566.

14 H. M. Kim and B. R. Cho, Small-Molecule Two-Photon Probes for Bioimaging Applications, *Chem. Rev.*, 2015, **115**, 5014–5055.

15 G. Bort, T. Gallavardin, D. Ogden and P. I. Dalko, From One-Photon to Two-Photon Probes: "Caged" Compounds, Actuators, and Photoswitches, *Angew. Chem. Int. Ed.*, 2013, **52**, 4526–4537.

16 L. Donato, A. Mourot, C. M. Davenport, C. Herbivo, D. Warther, J. Léonard, F. Bolze, J.-F. Nicoud, R. H. Kramer, M. Goeldner and A. Specht, Water-Soluble, Donor–Acceptor Biphenyl Derivatives in the 2-(o-Nitrophenyl)propyl Series: Highly Efficient Two-Photon Uncaging of the Neurotransmitter γ-Aminobutyric Acid at λ=800 nm, *Angew. Chem. Int. Ed.*, 2012, **51**, 1840–1843.

17 K. M. Schelkle, T. Griesbaum, D. Ollech, S. Becht, T. Buckup, M. Hamburger and R. Wombacher, Light-Induced Protein Dimerization by One- and Two-Photon Activation of Gibberellic Acid Derivatives in Living Cells, *Angew. Chem. Int. Ed.*, 2015, **54**, 2825–2829.

18 Q. Lin, L. Yang, Z. Wang, Y. Hua, D. Zhang, B. Bao, C. Bao, X. Gong and L. Zhu, Coumarin Photocaging Groups Modified with an Electron-Rich Styryl Moiety at the 3-Position: Long-Wavelength Excitation, Rapid Photolysis, and Photobleaching, *Angew. Chem. Int. Ed.*, 2018, **57**, 3722–3726.

19 K. A. Korzycka, P. M. Bennett, E. J. Cueto-Diaz, G. Wicks, M. Drobizhev, M. Blanchard-Desce, A. Rebane and H. L. Anderson, Two-photon sensitive protecting groups operating via intramolecular electron transfer: uncaging of GABA and tryptophan, *Chem. Sci.*, 2015, **6**, 2419–2426.

20 E. Cueto Diaz, S. Picard, M. Klausen, V. Hugues, P. Pagano, E. Genin and M. Blanchard-Desce, Cooperative Veratryle and Nitroindoline Cages for Two-Photon Uncaging in the NIR, *Chem. Eur. J.*, 2016, **22**, 10848–10859.

21 J. P. Olson, H.-B. Kwon, K. T. Takasaki, C. Q. Chiu, M. J. Higley, B. L. Sabatini and G. C. R. Ellis-Davies, Optically Selective Two-Photon Uncaging of Glutamate at 900 nm, *J. Am. Chem. Soc.*, 2013, **135**, 5954–5957.

22 J. P. Olson, M. R. Banghart, B. L. Sabatini and G. C. R. Ellis-Davies, Spectral Evolution of a Photochemical Protecting Group for Orthogonal Two-Color Uncaging with Visible Light, *J. Am. Chem. Soc.*, 2013, **135**, 15948–15954.

23 J. W. Johnson and P. Ascher, Glycine potentiates the NMDA response in cultured mouse brain neurons, *Nature*, 1987, **325**, 529–531.

Please do not adjust margins

Please do not adjust margins

24 R. S. Givens, M. Rubina and J. Wirz, Applications of p-hydroxyphenacyl (pHP) and coumarin-4-ylmethyl photoremovable protecting groups, *Photochem. Photobiol. Sci.*, 2012, **11**, 472–488.

25 V. Hagen, B. Dekowski, V. Nache, R. Schmidt, D. Geißler, D. Lorenz, J. Eichhorst, S. Keller, H. Kaneko, K. Benndorf and B. Wiesner, Coumarinylmethyl Esters for Ultrafast Release of High Concentrations of Cyclic Nucleotides upon One- and Two-Photon Photolysis, *Angew. Chem. Int. Ed.*, 2005, **44**, 7887–7891.

23 G. P. Hess, B. K. Carpenter, V. Shembekar and Y. Chen, US2007243519 (A1), 2007.

27 L. Fournier, I. Aujard, T. Le Saux, S. Maurin, S. Beaupierre, J.-B. Baudin and L. Jullien, Coumarinylmethyl Caging Groups with Redshifted Absorption, *Chem. Eur. J.*, 2013, **19**, 17494–17507.

28 Y. Chitose, M. Abe, K. Furukawa and C. Katan, Design, Synthesis, and Reaction of π-Extended Coumarin-based New Caged Compounds with Two-photon Absorption Character in the Near-IR Region, *Chem. Lett.*, 2016, **45**, 1186–1188.

29 M.-S. Schiedel, C. A. Briehn and P. Bäuerle, Single-Compound Libraries of Organic Materials: Parallel Synthesis and Screening of Fluorescent Dyes, *Angew. Chem. Int. Ed.*, 2001, **40**, 4677–4680.

30 J. Yu and Y. Shirota, A New Class of High-Performance Red-Fluorescent Dyes for Organic Electroluminescent Devices, [7-Diethylamino-3-(2-thienyl)chromen-2-ylidene]-2,2-dicyanovinylamine and {10-(2-Thienyl)-2,3,6,7-tetrahydro-1H,5H-chromeno[8,7,6-ij]quinolizin-11-ylidene}-2,2-dicyanovinylamine, *Chem. Lett.*, 2002, **31**, 984–985.

31 A. Gandioso, S. Contreras, I. Melnyk, J. Oliva, S. Nonell, D. Velasco, J. García-Amorós and V. Marchán, Development of Green/Red-Absorbing Chromophores Based on a Coumarin Scaffold That Are Useful as Caging Groups, *J. Org. Chem.*, 2017, **82**, 5398–5408.

32 M. Barzoukas and M. Blanchard-Desce, Molecular engineering of push–pull dipolar and quadrupolar molecules for two-photon absorption: A multivalence-bond states approach, *The Journal of Chemical Physics*, 2000, **113**, 3951–3959.

33 K. D. Belfield, A. R. Morales, B.-S. Kang, J. M. Hales, D. J. Hagan, E. W. Van Stryland, V. M. Chapela and J. Percino, Synthesis, Characterization, and Optical Properties of New Two-Photon-Absorbing Fluorene Derivatives, *Chem. Mater.*, 2004, **16**, 4634–4641.

31 G. H. Mcgall and A. D. Barone, US2011028350 (A1), 2011.

35 P. Stegmaier, J. M. Alonso and A. del Campo, Photoresponsive Surfaces with Two Independent Wavelength-Selective Functional Levels, *Langmuir*, 2008, **24**, 11872–11879.

36 G. A. Molander and M. R. Rivero, Suzuki Cross-Coupling Reactions of Potassium Alkenyltrifluoroborates, *Org. Lett.*, 2002, **4**, 107–109.

37 J. J. Smith, D. Best and H. W. Lam, Copper-catalyzed borylative coupling of vinylazaarenes and N-Boc imines, *Chem. Commun.*, 2016, **52**, 3770–3772.

38 T. Jeffery, On the efficiency of tetraalkylammonium salts in Heck type reactions, *Tetrahedron*, 1996, **52**, 10113–10130.

39 C. Bao, G. Fan, Q. Lin, B. Li, S. Cheng, Q. Huang and L. Zhu, Styryl Conjugated Coumarin Caged Alcohol: Efficient Photorelease by Either One-Photon Long Wavelength or Two-Photon NIR Excitation, *Org. Lett.*, 2012, **14**, 572–575.

40 M. Petit, C. Tran, T. Roger, T. Gallavardin, H. Dhimane, F. Palma-Cerda, M. Blanchard-Desce, F. C. Acher, D. Ogden and P. I. Dalko, Substitution Effect on the One- and Two-photon Sensitivity of DMAQ "Caging" Groups, *Org. Lett.*, 2012, **14**, 6366–6369.

41 S. Picard, E. Genin, G. Clermont, V. Hugues, O. Mongin and M. Blanchard-Desce, Octupolar chimeric compounds built from quinoline caged acetate moieties: a novel approach for 2-photon uncaging of biomolecules, *New J. Chem.*, 2013, **37**, 3899–3913.

42 S. R. Adams, J. P. Y. Kao, G. Grynkiewicz, A. Minta and R. Y. Tsien, Biologically useful chelators that release Ca2+ upon illumination, *J. Am. Chem. Soc.*, 1988, **110**, 3212–3220.

43 T. Šolomek, J. Wirz and P. Klán, Searching for Improved Photoreleasing Abilities of Organic Molecules, *Acc. Chem. Res.*, 2015, **48**, 3064–3072.

44 Y. Zhao and D. G. Truhlar, The M06 suite of density functionals for main group thermochemistry, thermochemical kinetics, noncovalent interactions, excited states, and transition elements: two new functionals and systematic testing of four M06-class functionals and 12 other functionals, *Theor Chem Account*, 2008, **120**, 215–241.

45 B. Schade, V. Hagen, R. Schmidt, R. Herbrich, E. Krause, T. Eckardt and J. Bendig, Deactivation Behavior and Excited-State Properties of (Coumarin-4-yl)methyl Derivatives. 1. Photocleavage of (7-Methoxycoumarin-4-yl)methyl-Caged Acids with Fluorescence Enhancement, *J. Org. Chem.*, 1999, **64**, 9109–9117.

46 R. Schmidt, D. Geissler, V. Hagen and J. Bendig, Kinetics Study of the Photocleavage of (Coumarin-4-yl)methyl Esters, *J. Phys. Chem. A*, 2005, **109**, 5000–5004.

47 A. Fischer, C. Cremer and E. H. K. Stelzer, Fluorescence of coumarins and xanthenes after two-photon absorption with a pulsed titanium–sapphire laser, *Appl. Opt., AO*, 1995, **34**, 1989–2003.

48 F. Terenziani, M. Morone, S. Gmouh and M. Blanchard-Desce, Linear and Two-Photon Absorption Properties of Interacting Polar Chromophores: Standard and Unconventional Effects, *ChemPhysChem*, 2006, **7**, 685–696.

49 A. S. Melnikov, P. Y. Serdobintsev, A. D. Vedyaykin and M. A. Khodorkovskii, Two-photon absorption cross section for Coumarins 102, 153 and 307, *J. Phys.: Conf. Ser.*, 2017, **917**, 062029.

50 The extrapolated δ_u value for DEAC450, determined from measurements conducted in MeCN/H2O (90/10, v/v) is two orders larger than the one reported in the literature for direct δ_u measurements conducted in biological medium. Although the 2PA response of DEAC450 was found to depend on the solvent (see SI), this could not account for such a discrepancy. Our study suggests that the reported δ_u value for DEAC450 may be significantly underestimated, making it one of the best 2P uncagers currently available.

51 J. Tomasi, B. Mennucci and R. Cammi, Quantum Mechanical Continuum Solvation Models, *Chem. Rev.*, 2005, **105**, 2999–3094.

52 T. Le Bahers, C. Adamo and I. Ciofini, A Qualitative Index of Spatial Extent in Charge-Transfer Excitations, *J. Chem. Theory Comput.*, 2011, **7**, 2498–2506.

53 D. Jacquemin, T. L. Bahers, C. Adamo and I. Ciofini, What is the "best" atomic charge model to describe through-space charge-transfer excitations?, *Phys. Chem. Chem. Phys.*, 2012, **14**, 5383–5388.

54 M. J. Frisch, G. W. Trucks, H. B. Schlegel, G. E. Scuseria, M. A. Robb, J. R. Cheeseman, G. Scalmani, V. Barone, B. Mennucci, G. A. Petersson, H. Nakatsuji, M. Caricato, X. Li, H. P. Hratchian, A.

 This journal is © The Royal Society of Chemistry 20xx

Please do not adjust margins

Please do not adjust margins

F. Izmaylov, J. Bloino, G. Zheng, J. L. Sonnenberg, M. Hada, M. Ehara, K. Toyota, R. Fukuda, J. Hasegawa, M. Ishida, T. Nakajima, Y. Honda, O. Kitao, H. Nakai, T. Vreven, J. A. Montgomery, Jr., J. E. Peralta, F. Ogliaro, M. Bearpark, J. J. Heyd, E. Brothers, K. N. Kudin, V. N. Staroverov, R. Kobayashi, J. Normand, K. Raghavachari, A. Rendell, J. C. Burant, S. S. Iyengar, J. Tomasi, M. Cossi, C. Rega, J. M. Millam, M. Klene, J. E. Knox, J. B. Cross, V. Bakken, C. Adamo, J. Jaramillo, R. Gomperts, R. E. Stratmann, O. Yazyev, A. J. Austin, R. Cammi, C. Pomelli, J. W. Ochterski, R. L. Martin, K. Morokuma, V. G. Zakrzewski, G. A. Voth, P. Salvador, J. J. Dannenberg, S. Dapprich, A. D. Daniels, Farkas, J. B. Foresman, J. V. Ortiz, J. Cioslowski and D. J. Fox, *Gaussian 09 revision D01*, Gaussian Inc. Wallingford CT 2009.

This journal is © The Royal Society of Chemistry 20xx

Please do not adjust margins